Mouse *Slc9a8* Mutants Exhibit Retinal Defects Due to Retinal Pigmented Epithelium Dysfunction

Shalini Jadeja,[1] Alun R. Barnard,[2] Lisa McKie,[1] Sally H. Cross,[1] Jacqueline K. White,[3] on behalf of the Sanger Mouse Genetics Project, Morag Robertson,[1] Peter S. Budd,[1] Robert E. MacLaren,[2] and Ian J. Jackson[1,4]

[1]MRC Human Genetics Unit, MRC Institute of Genetics & Molecular Medicine, University of Edinburgh, Edinburgh, United Kingdom
[2]Nuffield Laboratory of Ophthalmology, Nuffield Department of Clinical Neurosciences, University of Oxford, The John Radcliffe Hospital, Oxford, United Kingdom
[3]Wellcome Trust Sanger Institute, Wellcome Trust Genome Campus, Hinxton, Cambridge, United Kingdom
[4]Roslin Institute, University of Edinburgh, Edinburgh, United Kingdom

Correspondence: Ian J. Jackson, MRC Human Genetics Unit, Institute for Genetics and Molecular Medicine, University of Edinburgh, Crewe Road, Edinburgh EH4 2XU, UK; ian.jackson@igmm.ed.ac.uk.

Submitted: September 24, 2014
Accepted: February 19, 2015

Citation: Jadeja S, Barnard AR, McKie L, et al. Mouse *Slc9a8* mutants exhibit retinal defects due to retinal pigmented epithelium dysfunction. *Invest Ophthalmol Vis Sci*. 2015;56:3015–3026. DOI:10.1167/iovs.14-15735

Purpose. As part of a large scale systematic screen to determine the effects of gene knockout mutations in mice, a retinal phenotype was found in mice lacking the *Slc9a8* gene, encoding the sodium/hydrogen ion exchange protein NHE8. We aimed to characterize the mutant phenotype and the role of sodium/hydrogen ion exchange in retinal function.

Methods. Detailed histology characterized the pathological consequences of *Slc9a8* mutation, and retinal function was assessed by electroretinography (ERG). A conditional allele was used to identify the cells in which NHE8 function is critical for retinal function, and mutant cells analyzed for the effect of the mutation on endosomes.

Results. Histology of mutant retinas reveals a separation of photoreceptors from the RPE and infiltration by macrophages. There is a small reduction in photoreceptor length and a mislocalization of visual pigments. The ERG testing reveals a deficit in rod and cone pathway function. The RPE shows abnormal morphology, and mutation of *Slc9a8* in only RPE cells recapitulates the mutant phenotype. The NHE8 protein localizes to endosomes, and mutant cells have much smaller recycling endosomes.

Conclusions. The NHE8 protein is required in the RPE to maintain correct regulation of endosomal volume and/or pH which is essential for the cellular integrity and subsequent function of RPE.

Keywords: mouse model, retinal degeneration, retinal pigment epithelium, sodium-hydrogen exchange

In an international effort to assign function to all genes, and to identify new models of human disease, cohorts of mice produced from mutant embryonic stem cells are being screened in large-scale phenotyping pipelines. Hundreds of mouse lines, each mutant for a different gene, have been analyzed for developmental, hematological, immunological, metabolic, neurological, reproductive, and sensory parameters, which, thus, provide a comprehensive assessment of the consequences of gene ablation.[1] Included in the sensory analysis is slit-lamp examination of the anterior chamber of the eye, and indirect ophthalmoscopy to view the retina and retinal vessels. The phenotype data can be viewed online and the mice are freely available. We describe here the detailed pathological and functional analysis of a mouse line mutant in the sodium/hydrogen ion exchange protein gene, *Slc9a8*, which was identified as having a retinal defect and no other abnormality other than male sterility.

Sodium/hydrogen ion exchange proteins (NHEs) or cotransporter solute channels are encoded by the *Slc9* gene family, comprising nine members: *Slc9a1-9*, encoding NHE1-9. Proteins NHE1 to 5 are located in the plasma membrane while NHE6 to 9 are found in membranes of cell organelles (reviewed previously[2]). These proteins contain 12 membrane spanning domains and catalyze the electroneutral transport of cations down a concentration gradient. Typically sodium ions are transported in and hydrogen ions out of the cell or organelle. Simultaneous transport of anions creates osmotic pressure and results in influx of water, regulating the pH and volume of cells and organelles.

Sodium/hydrogen ion exchange is involved in aqueous humor dynamics and maintenance of intraocular pressure (IOP). Inhibition of sodium/hydrogen ion exchange in mice[3] reduces IOP and at least one cotransporter, NHE1, is found expressed in the ciliary body, where aqueous dynamics are regulated. The single yeast NHE is necessary for correct sorting of proteins to the vacuole[4] and, indeed, depletion of NHE8 in mammalian cells disrupts endosome trafficking.[5] Six of the *Slc9* family members have been mutated in mice and give rise to a range of phenotypes, from hyperactivity or ataxia and seizures (*Slc9a1* and *6*)[6–8] to relatively mild gastric secretion and absorption defects (*Slc9a2*, *3*, and *4*).[9–11]

The gene *Slc9a8* is widely expressed in adult mouse tissues, but is enriched in kidney, intestine, muscle, liver, and testes.[12,13] The gene is expressed in the kidney proximal

tubules, where reabsorption of secreted bicarbonate requires NHE function, although this is mostly via Slc9a3 (NHE3). However, *Slc9a8* is expressed at higher levels in the neonatal kidney, and may partially compensate for NHE3 in *Slc9a3* knockout animals, which have only a mild absorption defect.[14] The *Slc9a8* gene previously has been knocked out and the authors report that the mice have normal levels of serum sodium ions. They also report an increase in the length of the intestine, but a reduction in the number of goblet cells in the mutant mice with a concomitant reduction in mucin secretion and pH.[13,15] Furthermore, it has been reported recently that the gene is expressed in the epithelial cells of the conjunctiva, cornea, and lacrimal glands and may have a role in the protection of these ocular epithelia.[16] The male mutants also are sterile.

Here, we identified and characterized a previously undescribed retinal defect of *Slc9a8* knockout mice and located the origin of the phenotype to be abnormalities in the retinal pigmented epithelium.

Materials and Methods

Animals

The *Slc9a8*$^{tm1a(KOMP)Wtsi}$ mutant mice were obtained from the Wellcome Trust Sanger Institute (WTSI), which were generated as part of the Eumodic phenotyping screen. We maintained the mice on a C57BL6/J background. Germline Cre expressing mice were made by DJ Kleinjan, MRC Human Genetics Unit,[17] tyrosinase Cre expressing mice were from Lionel Larue, Institut Pasteur,[18] and R26MTMG reporter mice originally from Liqun Luo, Stanford University.[19] The FLPe expressing mice were made by Andrew Smith, University of Edinburgh.[20] All experiments complied with the ARVO Statement for the Use of Animals in Ophthalmic and Vision Research and the relevant local animal welfare conditions. Mice were genotyped by PCR using the primers in Supplementary Table S1.

RNA Expression

The RNA was prepared from adult eyes using the RNeasy Plus Mini kit (Qiagen, Venlo, The Netherlands) following the manufacturer's instructions. First strand cDNA was prepared from 300 ng RNA using the First Strand cDNA Synthesis Kit for RT-PCR (AMV; Hoffmann-La Roche, Basel, Switzerland) following the manufacturer's instructions. A total of 5% of this was used as a template for PCR using DreamTaq Green DNA Polymerase (Thermo Fisher Scientific, Waltham, MA, USA) with primers at 200 nM. The PCR amplification conditions used were as follows. One cycle of 94°C for 4 minutes, followed by 30 cycles of 94°C for 30 minutes, 58°C for 30 minutes, 72°C for 30 minutes, followed by one cycle of 72°C for 10 minutes. The PCR products were analyzed on 2% agarose gels. Primers used are in Supplementary Table S2.

Electroretinography (ERG)

Before testing, mice were dark adapted overnight (>18 hours) and anesthetized via intraperitoneal injection (80 mg/kg ketamine and 10 mg/kg xylazine). Pupils were dilated with 1% tropicamide and 2.5% phenylephrine eye drops. A DTL-type silver-coated nylon thread active electrode was modified to include a custom-made contact lens of clear Aclar film. This was positioned concentrically on the cornea using hypromellose eye drops (1% methylcellulose solution) for coupling. Platinum needles in the scruff and at the base of the tail served as reference and ground electrodes, respectively. Animals were maintained at 37°C using a heated blanket with feedback rectal probe. Signals were differentially amplified and digitized at a rate of 5 kHz using an Espion E2 console (Diagnosys LLC, Cambridge, UK) that controlled the timing of the light stimulus generated by a Grass PS33 photic stimulator dome. The intensity of the unattenuated, brief (10 μs), bright, white single-flash was 1.03 log lumen s/m^2. This was attenuated using neutral density filters to generate the dim flash (−2.57 log lumen s/m^2). Interstimulus intervals were 6 and 60 seconds for dim and bright flashes, respectively. Averaging of 16 and 4 flashes was used for dim and bright stimuli, respectively. For light-adapted recordings, animals were exposed to a steady white background (~150 lux) for 10 minutes, after which flashes of the bright stimulus were superimposed at a rate of 1 Hz with 20 flashes averaged per response.

Confocal Scanning Laser Ophthalmoscope Imaging

Imaging was performed using a Spectralis HRA confocal scanning laser ophthalmoscope (Heidelberg Engineering, Heidelberg, Germany). Mice were anesthetized and eyes dilated as above. A custom made polymethylmethacrylate (PMMA) contact lens was placed on the cornea with 0.3% methylcellulose gel as viscous coupling fluid. The mouse was positioned on a platform mounted on the chin rest of the cSLO device. All images were recorded using the 55° lens. The NIR reflectance image (820 nm diode laser) was used to align the fundus camera relative to the pupil and to focus on the confocal plane of interest. Fluorescence was excited using a 488 nm argon laser or a 790 nm diode laser and emission was recorded at 500 to 700 or greater than 810 nm, respectively. Images were recorded using "automatic real time" (ART) mode, which tracks ocular movement (e.g., due to respiration) and averages consecutive images resulting in an improved signal-to-noise ratio.

Color Fundus Imaging

Images of the fundus were collected by using a topical endoscope (BERCI Tele-Otoscope with HOPKINS straight forward 0°, diameter 3 mm, Halogen cold light fountain light source) and camera (Nikon D40x with Nikon AF 85mm F1.8D AF Nikkor lens; Nikon Corporation, Tokyo, Japan).

Tissue Preparation and Staining

Mice were killed at the appropriate age, and the eyes were enucleated and fixed in Davidson's fixative (28.5% ethanol, 2.2% neutral buffered formalin, 11% glacial acetic acid) overnight at 4°C. The eyes then were dehydrated through an ethanol series and embedded in paraffin for 7 μm sectioning on a Leica RM 2235 microtome for histological analysis (Leica, Wetzlar, Germany). Hematoxylin and eosin staining was performed according to standard procedures.

Immunofluorescence

Citrate buffer antigen retrieval was used for paraffin sections. We blocked all the sections in 10% heat inactivated donkey serum in PBS plus 3% Triton X-100 for an hour, and performed all antibody incubations in the same solution at room temperature for an hour in block or overnight at 4°C.

Whole mount RPE was dissected from unfixed eyes and then fixed in cold (−20°C) methanol for at least 30 minutes before immunofluorescence staining. Whole mount buffer (3% Triton X-100, 0.5% Tween-20, 1% BSA in PBS) was used to block, wash, and for all antibody incubations. Briefly, RPE was rehydrated in PBS, blocked for an hour, and primary antibodies

Investigative Ophthalmology & Visual Science

incubated at room temperature overnight. Following washes, secondary antibodies were incubated for 2 hours, washed in whole mount buffer twice, and PBS twice before being mounted and imaged.

Tissue from at least five mice of each genotype from at least three different litters was used for all analysis. All tissues were mounted in Vectashield (Vector Laboratories, Peterborough, UK), imaged by confocal microscopy (Nikon A1R; Nikon Corporation), and maximum intensity projections of z-stacks were created using NisElements AR Version 4.0 software. All images are representative of at least three animals.

For immunofluorescence, the following antibodies were used; rabbit anti-Slc9a8 (1:200; AbD Serotec, Kidlington, UK), mouse anti-rhodopsin (1:500; Merck Millipore UK Ltd., Watford, UK), rat anti-F4/80 (1:500; AbD Serotec, UK), rabbit anti-ML- Opsin (1:500; Merck Millipore), goat anti-S-opsin (1:500; Insight Biotechnology, Middlesex, UK), mouse anti-β-catenin (1:200; Sigma-Aldrich, Dorset, UK), rabbit-anti-ZO-1 (1:100; Invitrogen, Renfrew, UK), rat anti-transferrin receptor (1:200; Lifespan Biosciences, Inc., Seattle, WA, USA), and mouse anti-Golgin 97 (1:200; Invitrogen). Alexa Fluor secondary antibodies (1:500; Invitrogen) were used.

Retinal Thickness Measurement

Sections from 25-week-old mice were stained with hematoxylin and eosin and two images were taken from each eye near the center of the retina, adjacent to the optic nerve head, and two from the retinal periphery. For each image, 5 measurements of each retinal cell layer was taken using ImageJ.[21] A minimum of 5 eyes of each genotype were measured and the mean of these measurements was used.

IOP Measurement

The IOP measurements were obtained as described previously,[22] with modifications. The mice were anesthetized by intraperitoneal (IP) injection of a 0.1 mL/10 g bodyweight of a 100 mg/mL ketamine–10 mg/mL xylazine mixture. The rebound tonometer, TonoLab (Icare, Helsinki, Finland), was used to take a set of 6 measurements of IOP in each eye. The IOP measurements always were taken at the same time of day, between 1 PM and 3 PM. All cohorts included male and female mice. At 1 to 3 months 30 (wild-type) and 36 (homozygous) eyes measured, while at 3 to 6 months 28 eyes of each genotype measured.

Plasmid Construction

An NHE8-hemaglutinin construct was obtained[5] and the human *Slc9a8* coding region lacking the translation stop codon was cloned as a PCR fragment into XhoI-BamHI sites into the vector pmKATE2-N (Evrogen, Exeter, UK). The GalT-GFP TGN expression marker was obtained from Mark Handley (MRC HGU; Edinburgh, UK).

Cell Culture

Human RPE1 cells were grown in DMEM:F12 (Invitrogen) supplemented with 10% fetal calf serum (FCS) and 1% penicillin/streptomycin in a humidified 5% CO_2 incubator at 37°C. Mouse embryonic fibroblasts (MEFs) were isolated from E13.5 embryos. Embryo heads and organs were removed before trypsin digestion at room temperature for 30 minutes. Digested samples were plated in Optimem (Invitrogen) supplemented with 10% FCS, 1% penicillin/streptomycin, and 0.00074% β-mercaptoethanol in a humidified 5% CO_2, 3% O_2 incubator at 37°C. The RPE1 cells were transfected using Lipofectamine 2000 (Invitrogen) following the manufacturer's instructions. Cells were imaged live 48 hours after transfection in HBSS containing calcium and magnesium ions.

Organelle Volume and Intensity Measurements

We used 5 MEF lines of each genotype from 3 litters at passages 3 to 5 and they were plated at a density of 2×10^4 cells/well of a 24-well plate. At 48 hours following plating, FITC conjugated rat anti-transferrin receptor antibody was added to the growth medium at a dilution of 1:200 and incubated at room temperature for 30 minutes. The cells were washed and incubated in Hanks' balanced salt solution (HBSS) containing calcium and magnesium ions for imaging. For each MEF cell line a minimum of 10 independent images were taken. The Volocity 3D Image analysis software (PerkinElmer, Waltham, MA, USA) was used to quantify the number, volume, and mean FITC-intensity of each recycling endosome.

Results

Slc9a8 Mutant Mice Exhibit an Eye Phenotype

An international effort to produce "knockout" mutations of all the genes in the mouse genome has generated libraries of embryonic stem cells and mice containing targeted mutations. In many cases the vectors are designed to eliminate gene function ("knockout first"), but with the capability of engineering the allele in mice to produce a Cre-recombinase conditional allele, so that temporally or spatially restricted knockouts can be generated, and a more robust knockout mutation can be made by deleting a critical exon.[23] Mice carrying the "knockout first" mutant allele of *Slc9a8* (*Slc9a8*$^{tm1a(KOMP)Wtsi}$) were generated. In this allele exon 3 of *Slc9a8* splices onto *LacZ* in the targeting construct to generate a reporter-tagged mutation. We subsequently generated mice carrying the *Slc9a8*$^{tm1d(KOMP)Wtsi}$ allele, by sequential crossing with animals expressing the recombinases Flp and Cre in the germ line. In this allele the targeting cassette and the 59bp exon 4 are deleted, resulting in a frame-shift. Reverse-transcription PCR (RT-PCR) amplification of mRNA from wild-type, heterozygous, and homozygous mutant eyes shows that no *Slc9a8* mRNA is made in knockout first (tm1a) eyes (Fig. 1A). The RNA from eyes of exon 4 deleted (tm1d) mice produced amplification products smaller by 59 base pairs (bp), indicating transcription of the internally deleted, frameshift, mRNA (Fig. 1A).

Mice homozygous for the knockout first allele were tested in the WTSI pipeline of phenotype assessments.[1] This battery of tests provides a first-pass analysis of a wide range of phenotypic parameters. The *Slc9a8* mutant mice are morphologically normal, and show no phenotypic deviation from wild-type in all but two tests (available in the public domain at http://www.mousephenotype.org/data/genes/MGI:1924281). Firstly, male mutant mice are almost completely infertile. From 25 matings between mutant males and females of either heterozygous or homozygous genotypes, 24 gave no offspring and one mating between a homozygous male and a heterozygous female produced a single litter with two pups. By contrast, 8 homozygous females mated with wild-type males produced 13 litters with a total of 87 pups (6.7 per litter), and a further 38 homozygous females mated with heterozygous males produced 445 pups in 65 litters (6.8 per litter). Three of these 46 females produced no offspring.

Secondly, all mutant mice examined by indirect ophthalmoscopy (7 male and 7 female) showed abnormal pigmentation of the retina (Figs. 2A, 2B). All homozygotes had many

Investigative Ophthalmology & Visual Science

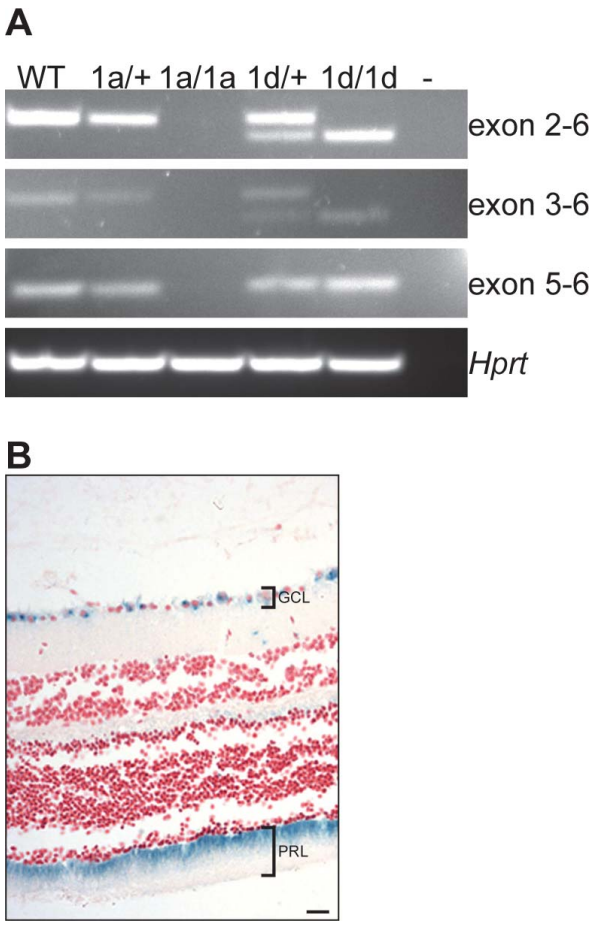

Figure 1. Expression of Slc9a8 in knock and wild-type eyes. The RT-PCR from adult eye samples (**A**) shows that *Slc9a8* is knocked out in the *Slc9a8*$^{tm1a(KOMP)Wtsi}$ and *Slc9a8*$^{tm1d(KOMP)Wtsi}$ alleles. Shown are RT-PCR products produced using primer pairs from exons 2 and 6, 3 and 6, 5 and 6 of *Slc9a8*, and 7 and 9 from *Hprt* as a control. Primer sequences are in Supplementary Table S2. Genotypes of samples are as follows; wild-type (WT), heterozygous *Slc9a8*$^{tm1a(KOMP)Wtsi}$ (1a/+), homozygous *Slc9a8*$^{tm1a(KOMP)Wtsi}$ (1a/1a), heterozygous *Slc9a8*$^{tm1d(KOMP)Wtsi}$ (1d/+), homozygous *Slc9a8*$^{tm1d(KOMP)Wtsi}$ (1d/1d), no template (-). (**B**) Section of retina from heterozygous *Slc9a8*$^{tm1a(KOMP)Wtsi}$ mice, stained for β-galactosidase. *Blue stain* reveals expression in the photoreceptors (PRL) and retinal ganglion cells (GCL). *Scale bar*: 50 μm.

darkly pigmented patches throughout the retina, possibly indicative of retinal degeneration or abnormalities of the RPE. Mutant mice generated for this screen are produced on a genetic background, which is a mixture of C57BL6/J and C57BL6/N strains. The latter contains the *rd8* deletion mutation in the *Crb1* gene and which results in late onset retinal degeneration and abnormal retinal lamination.[24,25] Although *Crb1*^{rd8} mutants clearly differ from the *Slc9a8* mutant in retinal phenotype and age of onset, it was important that this mutation be removed to avoid confounding the analysis. Thus, we backcrossed the original strain onto C57BL6/J and identified mice that were wild-type at *Crb1*, but carried the *Slc9a8* mutation. Subsequent analyses were on mice without the *Crb1*^{rd8} mutation and on a C57BL6/J background.

The *Slc9a8* gene is widely expressed throughout many tissues. We examined the sites of expression of the gene in the eye by staining heterozygous knockout first eyes for expression of the β-galactosidase gene inserted into the locus. Figure 1B clearly shows blue staining of expression in the photoreceptors and the ganglion cells of the retina. Unfortunately, the melanin of the RPE (absent from Fig. 1B) obscures staining for expression in those cells.

To further analyze the retinal phenotype, we examined mutant eyes by scanning laser ophthalmoscopy (SLO). Infra-red (IR) reflectance imaging showed grainy and highly reflective dots in mutant retinas, which were not present in control mice (Figs. 2C, 2D). Autofluorescence (AF) imaging with a 488-nm laser revealed marked abnormalities in the mutant retina; uniform background AF appeared to be reduced compared to wild-type controls, but many small hyperautofluorescent puncta were present across the retina (Figs. 2E, 2F), perhaps suggesting the infiltration of autofluorescent macrophages into the retina and/or the activation of resident microglia. The AF imaging with the near infrared 790 nm laser again showed hyperautofluorescent puncta spread throughout the retina of mutant mice and also more extensive regions of hyper-autofluorescence (Figs. 2G, 2H). High 790 nm AF is likely indicative of RPE pathology in mutant mice. Puncta and patches of high 790 nm and 488 nm AF resided in the outermost retina/RPE and often, but not always, colocalized.

Retinal Histology of *Slc9a8* Mutant Mice

We investigated the retinal pathology in more detail by examining histological sections. The most striking histopathological change was in the RPE. While wild-type sections show close apposition between the RPE and the neural retina, mutant retinas have a distinct separation of these cell layers. Some areas have wide detachment, which may be an artefact of sample preparation, but elsewhere, throughout the retina, there is a clear gap between the photoreceptors and the RPE (Figs. 3A–D). Within this space and penetrating far into the photoreceptor layer are many pigmented cells (white arrows, Figs. 3B, 3D). We investigated the identity of these cells by staining retinal sections of mutant mice with an antibody against the macrophage membrane protein F4/80, and counterstained for rhodopsin (Fig. 3E). Positive staining for F4/80 in the ectopic pigmented cells suggests they are macrophages, consistent with the observations by SLO. They are likely to have become pigmented by engulfing melanin or melanin-containing cells. Immunostaining shows they also contain rhodopsin, suggesting that they have engulfed photoreceptor outer segments (Fig. 3E).

The mutant retinas show some loss of photoreceptors, as indicated by a slight thinning of the outer nuclear layer (ONL). This was most pronounced in older mice (over 25 weeks of age), but even in these mice the reduction in ONL was no more than 16% (Supplementary Table S3, schematically shown in Fig. 3F). The photoreceptor outer segment layer also was thinner, indicating that although there has been some loss of these cells, there also is an overall shortening of the photoreceptors (Fig. 3G).

To investigate the effect of the mutation on rods and cones, we stained retinal sections with antibodies against rhodopsin and cone opsins (Figs. 4A–D). Rods and cones are affected in the mutant mice. The photoreceptor outer segments are shorter than normal and there appears to be a reduction in the number of cones, stained for cone opsins (Figs. 4A, 4B). In addition, there is a striking mislocalization of opsins within the cones (Figs. 4C, 4D).

RPE Morphology Is Abnormal in *Slc9a8* Mutant Mice

To examine the RPE in more detail, we prepared flat-mounts of this tissue and stained for ZO1, to examine the tight junctions between cells in this epithelium. In wild-type RPE, the cell

Investigative Ophthalmology & Visual Science

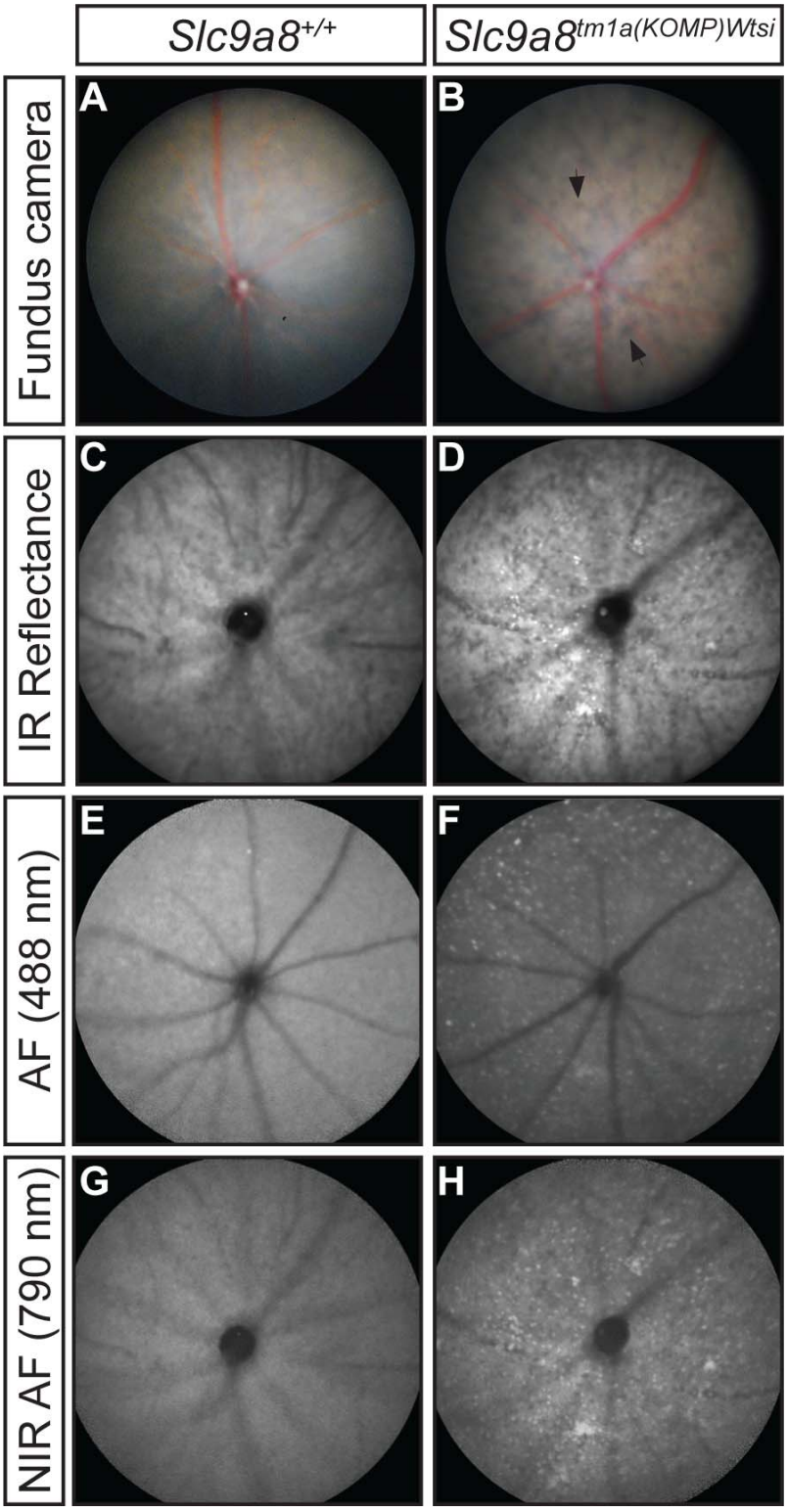

Figure 2. Retinal defects in *Slc9a8*$^{tm1a(KOMP)Wtsi}$ mice. Fundus image of a control retina (**A**) showing normal retinal morphology. Initial phenotyping by the Sanger Mouse Genetics Project identified retinal defects in *Slc9a8*$^{tm1a(KOMP)Wtsi}$ homozygous mutant mice, as evidenced by the presence of *dark patches* (*arrowheads*, [**B**]). (**C**–**H**) Scanning laser ophthalmoscope images of wild-type control (**C**, **E**, **G**) and *Slc9a8* mutant (**D**, **F**, **H**) eyes. (**C**, **D**) Infrared reflectance imaging. (**E**, **F**) Autofluorescence at 488 nm. (**G**, **H**) Autofluorescence at 790 nm.

junction staining reveals the typical hexagonal morphology of the RPE (Fig. 4E). The 4′6-dimidino-2-phenylindole (DAPI) staining for DNA shows some cells are binuclear, or two cells are within a single, hexagon of ZO1 deposition, but all lie within a regular and contiguous pattern. By contrast, in mutant RPE there are regions where numerous nuclei are seen enclosed within a large segment of ZO1, suggesting larger multinucleated cells (Fig. 4F). This suggests a loss of RPE cells

Investigative Ophthalmology & Visual Science

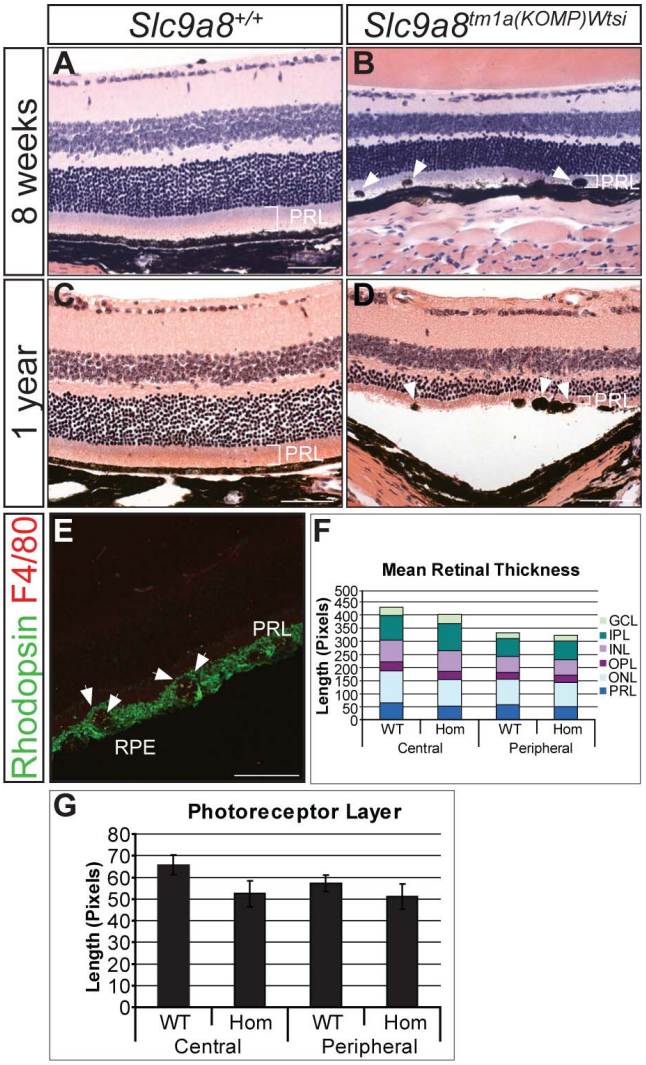

Figure 3. Retinal histology of *Slc9a8*$^{tm1a(KOMP)Wtsi}$ mice. Histological analysis of hematoxylin and eosin stained sections identified the onset of the degeneration at around 8 weeks. Control retinas show normal lamination (**A**) whereas *Slc9a8*$^{-}$ mutant retinas exhibit thinning of the PRL with infiltration of the RPE (*arrowheads*, [**B**]). By 1 year of age, control retinas (**C**) still show full thickness of the PRL, but mutant retinas (**D**) exhibit further thinning of this layer and continued RPE infiltration. Immunofluorescence shows positive staining for macrophages (F480) (*red*) containing rhodopsin (*green*) in the RPE infiltrates, suggesting phagocytosis of photoreceptors (**E**). Measurement of retinal cell layers shows a slight decrease in overall retinal thickness in the central and peripheral *Slc9a8* homozygous mutant (Hom) compared to WT controls (**F**). The decrease in the photoreceptor layer in the centre of the retina is statistically significant (1-way ANOVA, $^{*}P < 0.05$, [**G**]). Numerical data are in Supplementary Table S3. OPL, outer plexiform layer; INL, inner nuclear layer; IPL, inner plexiform layer (IPL). *Scale bars*: 50 μm.

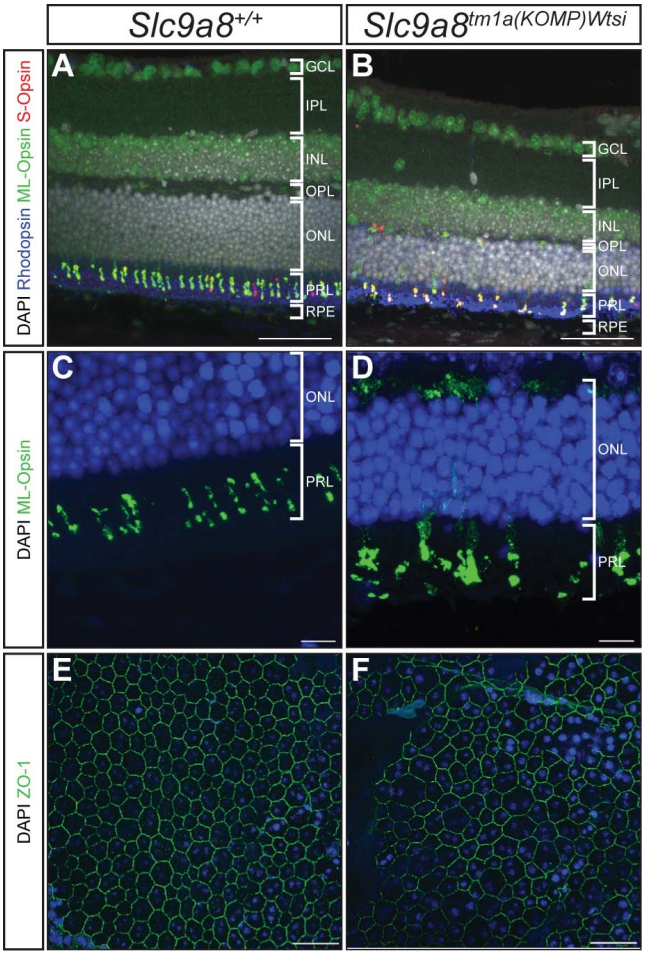

Figure 4. Characterization of retinal degeneration in *Slc9a8*$^{tm1a(KOMP)Wtsi}$ mutant mice. Immunofluorescence of a control retinal section shows regular expression of all three opsins (Rhodopsin, *blue*; ML-opsin, *green*; and S-opsin, *red*) (**A**). The *Slc9a8* mutant retinas shows reduced numbers of opsin-positive cells (**B**). Higher magnification shows the regular cone morphology in ML-opsin positive cells (*green*) in control retinas (**C**). Cone outer segments appear irregular in *Slc9a8* mutant mice with accumulation of ML-opsin in the nucleus and synapses (*green*, [**D**]). The RPE flat mounts stained with ZO-1 (*green*) show polygonal mononuclear cells in controls (**G**). The *Slc9a8* mutant RPE cells are more irregular with multinucleated cells (**H**). *Scale bars*: 50 μm (**A**, **B**, **E**, **F**), 10 μm (**C**, **D**).

as RPE cell death often is accompanied by the increase in size of the neighboring cells to prevent gaps appearing in the epithelium.[26]

Impaired Retinal Function in *Slc9a8* Mutant Mice

To examine retinal function we performed ERG in mutant ($n = 7$) and control ($n = 8$) mice at 23 to 25 weeks of age. Dark-adapted ERG responses were recorded to dim and bright flash stimuli; intensity-dependent responses could be seen in mutant mice, but there were clear deficits in the size and speed of responses when compared to wild-type animals (Fig. 5, data in Supplementary Table S4).

In dark-adapted conditions, the initial negative deflection of the ERG (the a-wave) is indicative of rod photoreceptor function. In mutant mice, the amplitude of the a-wave was significantly reduced in response to dim (Figs. 5A, 5B) and bright (Figs. 5D, 5E) stimuli. The time until the peak of the a-wave (implicit time) was significantly increased in mutant mice in response to the bright stimulus (Fig. 5E), although the timing of responses to dim stimuli was not significantly different (Fig. 5B).

Following the negative a-wave is a strong positive deflection known as the b-wave. The positive peak of the b-wave primarily reflects the activation of bipolar cells (second-order neurones that are immediately downstream of photorecep-

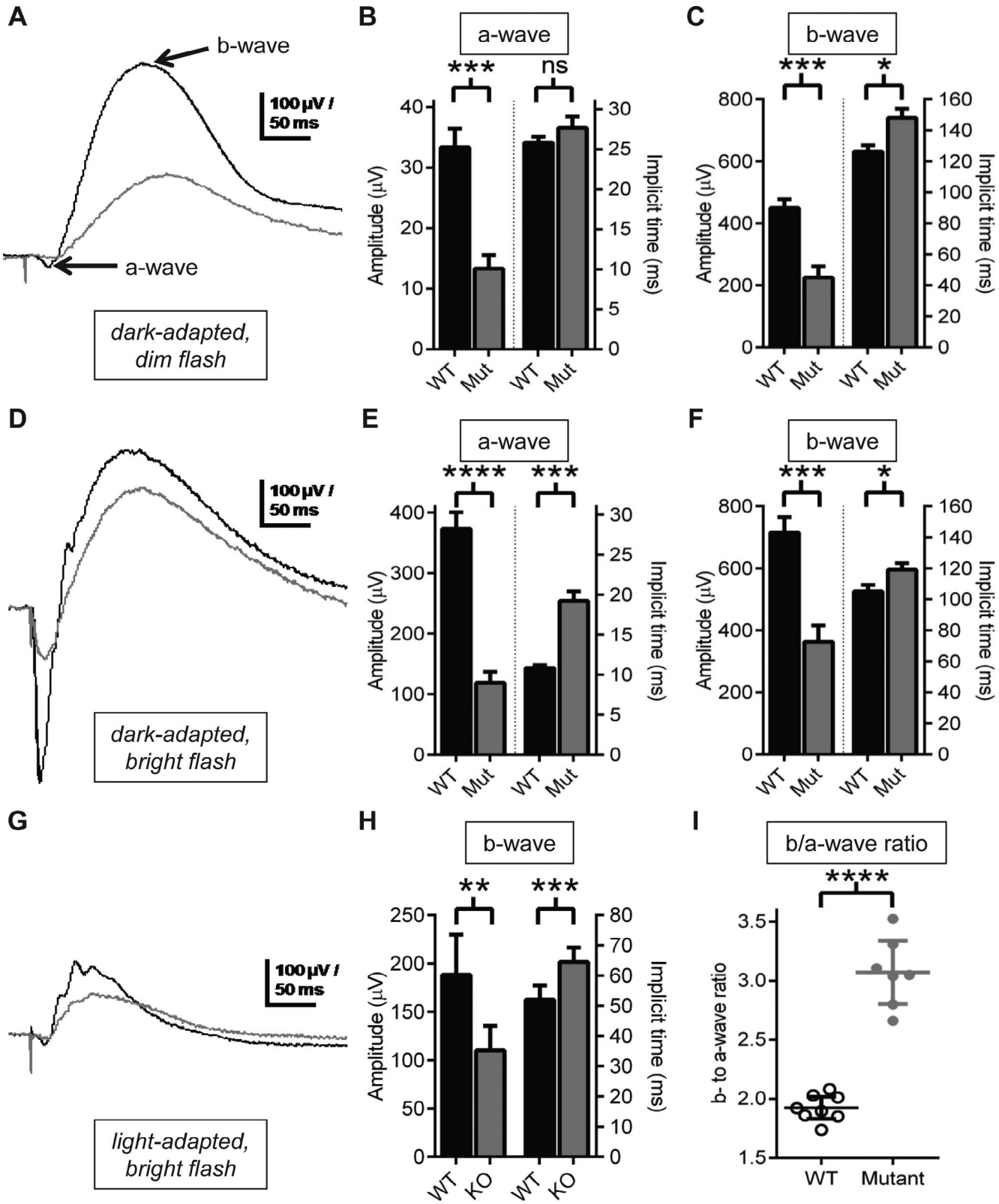

Figure 5. The ERG of *Slc9a8*$^{tm1a(KOMP)Wtsi}$ mutant mice (**A**, **D**, **G**). The ERGs of control (*black traces*) and *Slc9a8* mutant (*gray traces*) mice measuring rod responses in dark adapted mice (**A**, **D**) and cone responses in light-adapted mice (**G**). (**B**) The a-wave amplitude and implicit time of control and mutant mice in response to a dim flash. Amplitude shows a significant reduction in mutants, but the implicit time is not different. (**C**) The b-wave amplitude and implicit time of control and mutant mice in response to a dim flash. Amplitude shows a significant reduction in mutants and implicit time has a significant increase. (**E**) In response to a bright stimulus, mutant mice have a reduced a-wave amplitude and longer implicit time. (**F**) The b-wave amplitude and implicit time in response to a bright stimulus shows a decrease in amplitude and increase in implicit time. (**H**) The b-wave response of light adapted mice to a bright stimulus (cone pathway) shows mutant mice have a reduced amplitude and longer implicit time. Means, SEM, and statistics are in Supplementary Table S4. (**I**) Dark-adapted, bright flash b-wave to a-wave ratio is significantly higher in mutant

Investigative Ophthalmology & Visual Science

mice (3.070 ± 0.1097 mean ± SEM, $n = 7$) than in controls (1.925 ± 0.03967 mean ± SEM, $n = 8$; unpaired *t*-test with Welch's correction $P < 0.0001$, $t = 9.821$, df = 7.562). ns = $P > 0.05$, *$P \leq 0.05$, **$P \leq 0.01$, ***$P \leq 0.001$, ****$P \leq 0.0001$.

tors), particularly ON-type, depolarizing bipolar cells. By convention the magnitude of the b-wave is measured from the trough of the preceding a-wave, where present.

For this reason, a deficit in the a-wave will almost inevitably lead to a respective abnormality in the b-wave. Consequently, we observed a significantly smaller b-wave in mutant mice in dim (Fig. 5C) and in bright (Fig. 5F) flash conditions. Mutant mice also had slower b-waves; the implicit time of the b-wave was significantly increased in response to dim and bright stimuli (Figs. 5C, 5F).

Deficits in the size and speed of the b-wave might point to a defect in bipolar cell signalling and/or function. However, to distinguish between a disorder that is localized primarily to the photoreceptors and one that also impacts on more proximal retinal cells, it is important to consider the proportionality between a- and b-waves. Therefore, we calculated the size of the dark-adapted, bright flash ERG b-wave as a ratio of the a-wave amplitude recorded in the same individual (b/a-wave ratio). This revealed that in wild-types the ratio was 1.93 ± 0.04 (mean ± SEM, $n = 8$) and was increased by >50%, to 3.07 ± 0.11 (mean ± SEM, $n = 7$) in mutant mice (Fig. 5I). This highly significant increase ($P = 0.0001$, unpaired *t*-test with Welch's correction) suggests that bipolar cells are not directly affected by the mutation and there may even be some compensatory increase in the amplification of signal transmission in the outer plexiform layer.

To isolate retinal responses of the cone pathway, after dark-adapted recordings were finished, mice were exposed to a rod-saturating background illumination for at least 10 minutes and ERGs then were recorded for bright flash stimuli superimposed on the background. In these light-adapted conditions, the ERG response in mice is dominated by the positive b-wave and little or no negative a-wave is observed (Fig. 5G). Therefore, activity of cone photoreceptors cannot be directly recorded, but activation of ON bipolar cells of the cone pathway can be measured by the b-wave. In light-adapted ERG recordings, the responses of mutant mice were again significantly smaller and slower than wild-type controls. The amplitude of the b-wave was reduced by approximately 42% and the b-wave implicit time was increased by approximately 24% (Fig. 5H).

Overall, we found highly significant differences between mutant and wild-type animals, in terms of rod and cone pathway function (*P* values in Supplementary Table S4). In all tests, mutant ERG responses were smaller and slower than those of wild-type control animals. In particular, the ratio of b/a-wave amplitudes in dark-adapted ERGs points to a deficit in photoreceptor cells in mutant mice. When we examined histologically the eyes of mice that had undergone ERG testing, we found that, as before, photoreceptor cell number (as measured by ONL thickness) is only mildly reduced in mutant mice (data not shown). In general, the deficits in retinal function appear to be much greater than the retinal degeneration observed on histology (for example there is an approximately 68% reduction in the dark-adapted ERG, but only a <16% reduction in the ONL thickness). This indicates that the major cause of ERG abnormalities is not photoreceptor cell loss, but rather a substantial deficit in individual photoreceptor function. This is combined with a mild degree of photoreceptor cell loss, which could be caused as a primary result of the mutation or as a secondary consequence of impaired RPE function.

Slc9a8 Mutant Mice Have Normal IOP

Sodium hydrogen ion exchange is required to maintain the IOP, and inhibition of NHE function causes reduction in IOP. We considered the possibility that the retinal defect observed in *Sc9a8* mutant mice was secondary to a reduced IOP. We measured the IOP of mutant and control animals by tonometry and found that there was no difference in pressure between the two groups of mice (Supplementary Fig.).

RPE Specific Knockout of *Slc9a8* Results in Retinal Defects

To investigate the primary cause of the retinal pathology in *Slc9a8* mutant mice, we generated mice in which the gene was deleted only in the RPE, and not in the neural retina. This we achieved by initially converting the knockout first allele to a conditional allele (*Slc9a8*$^{tm1c(KOMP)Wtsi}$) by crossing with mice expressing a germ-line FLP-recombinase. This recombinase deletes the DNA between the *frt* sites, which flank the beta-geo selection cassette in the targeted allele to produce a gene with restored function, containing only *loxP* sites flanking exon 4. We confirmed that this allele functioned normally by examining the eyes of homozygous conditional mice in absence of Cre-recombinase, which we found to be unaffected (Figs. 6A, 6C). We then crossed these animals with mice carrying the *Tyr-Cre* transgene, which expresses Cre recombinase from the tyrosinase promoter, active in melanocytes and RPE cells. To confirm the tissue specificity of the *Tyr-Cre* we crossed it to mice with the *R26MTMG* transgene. This transgene expresses the fluorescent tomato protein in all cells, from the Rosa26 promoter, except in the presence of Cre recombinase when the tomato is deleted and the cells express green fluorescent protein instead.[19] Examination of the retinas of mice with the *Tyr-Cre* and *R26MTMG* transgene indicated that the Cre recombinase was only active in the RPE (which was green) and not in the neural retina (all layers of which were red, Fig. 6E).

By crossing mice with the conditional allele of *Slc9a8* with *Tyr-Cre* we generated animals that were homozygous for conditional *Slc9a8* and expressed Cre recombinase in the RPE. On examination of these eyes we found a phenotype indistinguishable from that with the constitutive knockout-first allele, by indirect ophthalmoscopy (Fig. 6B, compare to Fig. 2B) and by histology (Fig. 6C, compare to Figs. 3B, 3D). Note in particular the separation of RPE from the photoreceptors, and the presence of pigmented cells, probably macrophages containing engulfed melanin, in the photoreceptor layer, as seen in the global knockout phenotype in Figures 3B and 3D. We concluded that loss of *Slc9a8* in the RPE is sufficient to cause the histological retinal phenotype we observed, although we have not analyzed ERGs of these animals.

Loss of *Slc9a8* Results in Changes in Recycling Endosomes

One major function of the RPE in retinal physiology is in the visual cycle, whereby there is a transfer of retinals between photoreceptors and RPE with isomerization and reisomerization between 11-*cis* and all-*trans* retinal. A second important function is the phagocytosis of outer segment discs shed by

Investigative Ophthalmology & Visual Science

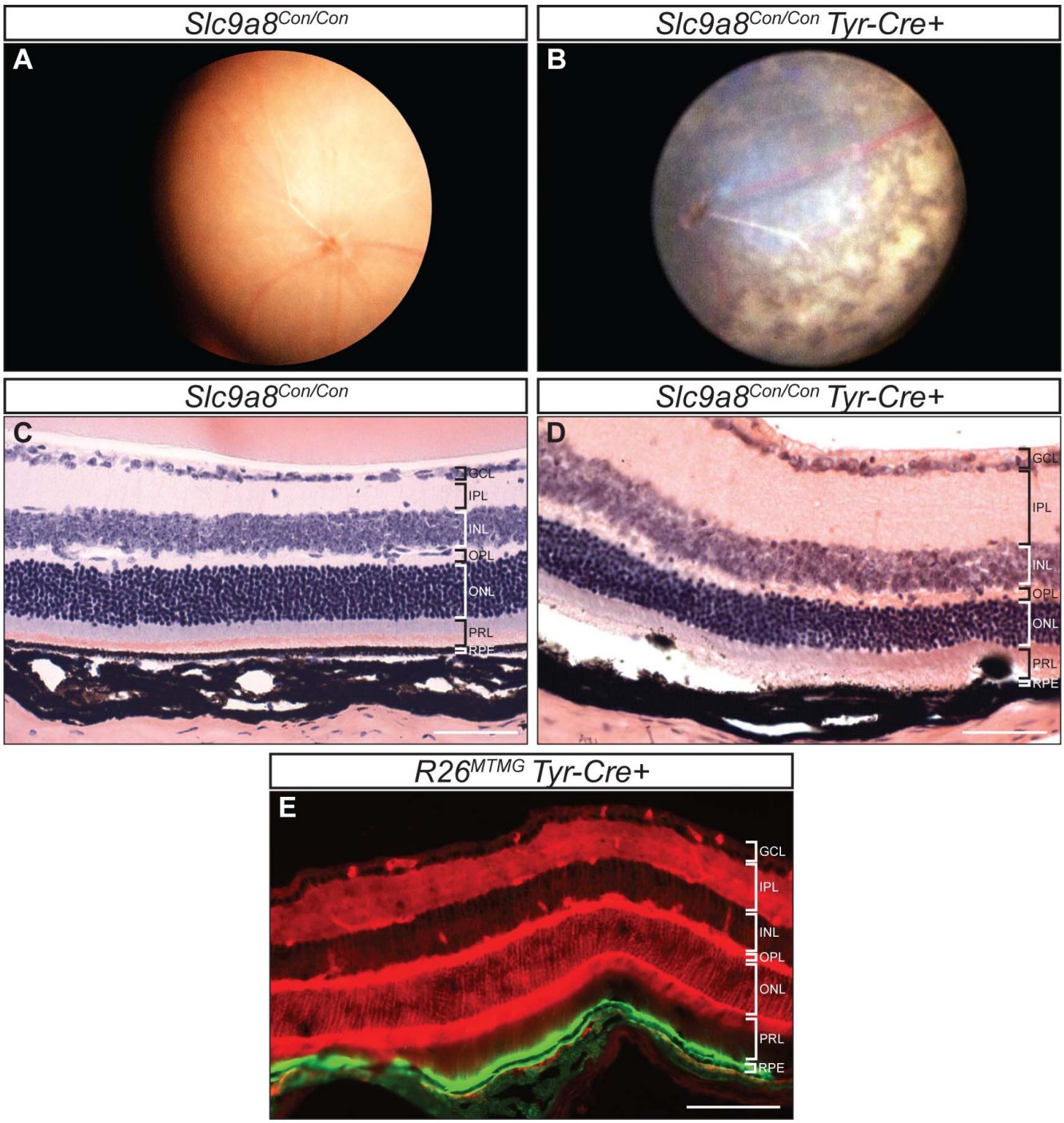

Figure 6. Loss of *Slc9a8* in the RPE Alone Causes the Mutant Phenotype. The *Slc9a8*$^{tm1a(KOMP)Wtsi}$ allele was converted to the conditional *Slc9a8*$^{tm1c(KOMP)Wtsi}$ (*Slc9a8*^{con}) allele by crossing with a mouse expressing Flpe in the germ line. Fundus imaging shows a normal appearance of the retina of homozygous *Slc9a8*^{con} mice (**A**). Retinal histology of a homozygous *Slc9a8*^{con} eye, hematoxylin and eosin stained, shows normal morphology (**C**). Fundus imaging of a retinas of 8-week-old mice homozygous for *Slc9a8*^{con} and hemizygous for the RPE-specific *Tyr-Cre* transgene shows the same phenotype as a constitutive knockout (**B**). Hematoxylin and eosin stained section of a retina from the mouse in (**B**), at 12 weeks, shows mutant retina produced by an RPE-specific knockout of *Slc9a8*. (**D**) We have analysed 4 mice that show the retinal phenotype from 2 separate litters. Fluorescence imaging of a retina from *R26*^{MTMG} mouse crossed with *Tyr-Cre* demonstrating activity of Cre only in the RPE (showing *green* fluorescent protein) and not in the other retinal layers (showing *red*, tomato, fluorescence, [**E**]). *Scale bars*: 50 μm (**A**, **C**) and 100 μm (**D**).

the photoreceptors. Both these functions require recycling endosomes in the RPE. Others have previously reported that the *Slc9a8* encoded protein (NHE8) localizes to the trans-Golgi network (TGN) and to late endosomes in HeLa cells, and that treatment of these cells with siRNA against *Slc9a8* results in an endosomal phenotype.[5] We confirmed this localization in RPE1 cells; NHE8 tagged with either HA for immune-detection, or with mKate for direct fluorescent imaging was found in the TGN (Figs. 7A–E). In agreement with others we also found NHE8 in late, (recycling)

Investigative Ophthalmology & Visual Science

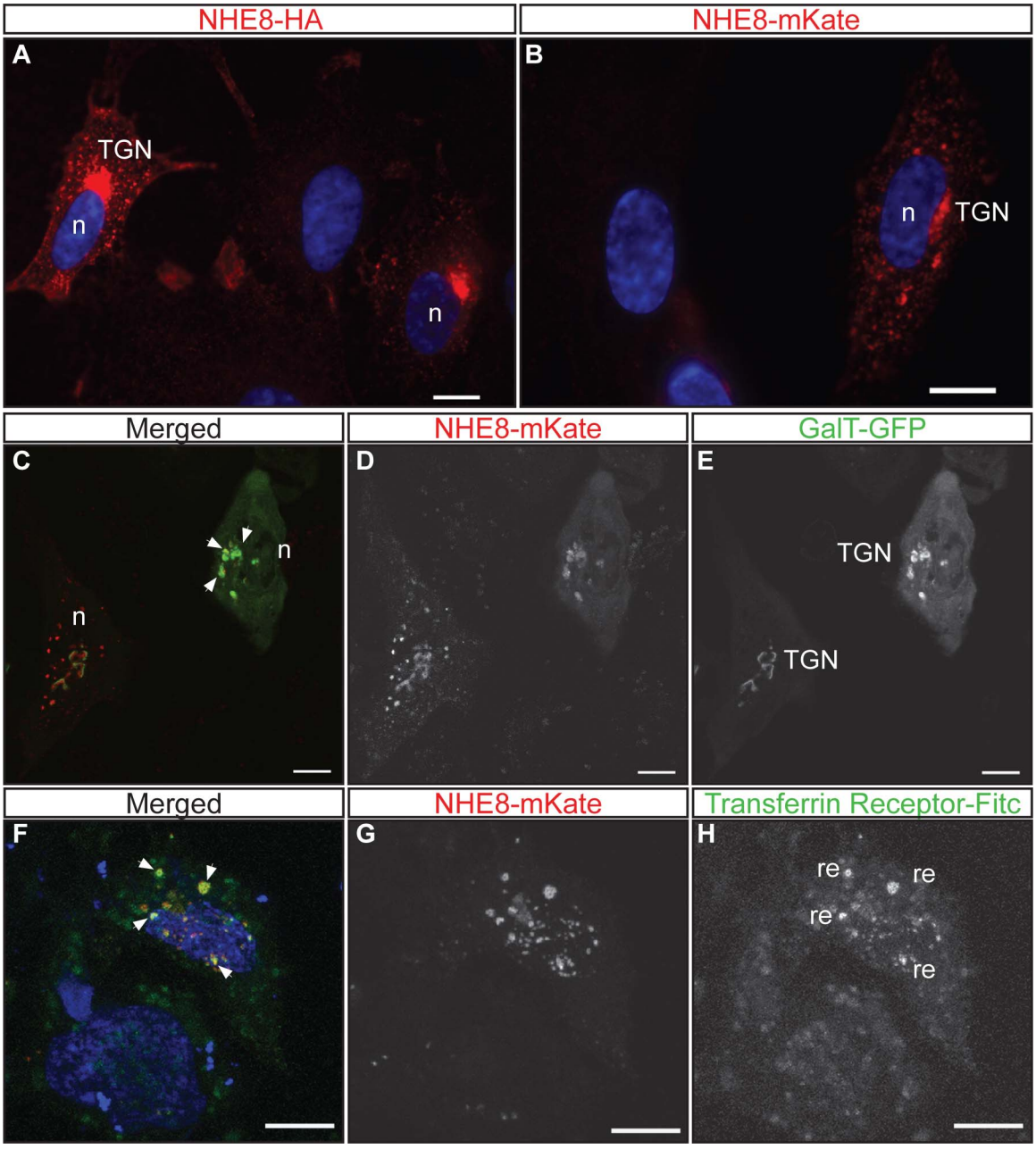

Figure 7. The NHE8 protein localizes to the trans-golgi network and recycling endosomes. (**A**) Localization of HA tagged NHE8 protein in RPE1 cells, previously demonstrated to be found in the trans Golgi network (TGN) of HeLa cells.[5] (**B**) The mKate-tagged NHE8 shows a similar pattern of localization in RPE1 cells. (**C–E**) The NHE8-mKate colocalizes with the TGN marker, GFP-tagged GalT (*arrows*) and (**F–H**) with the recycling endosome (re)marker transferrin receptor (*arrows*) (**F–H**). Nuclei demarked with "*n*". *Scale bars*: 10 μm.

endosomes, colocalized with transferrin receptor, in RPE1 cells (Figs. 7F–H).

To observe the effect of loss of *Slc9a8* on endosomes we isolated MEFs from wild-type and mutant embryos, and stained for golgin97 and transferrin receptor. Sodium/hydrogen ion cotransporters regulate pH and volume of organelles by affecting the distribution of ions. We measured the volume of recycling endosomes, stained with transferrin receptor antibodies, and found them to be reduced in size in mutant cells compared to wild-type. The mean volume per mutant endosome is approximately 50% that of the controls (Fig. 8, 1-way ANOVA, $P = 0.04$).

Discussion

Slc9a8$^{tm1a(KOMP)Wtsi}$ Mutant Mice Exhibit a Prominent Retinal Phenotype

We have shown here that mice lacking *Slc9a8* manifest a noticeable ocular phenotype, which consists of retinal degeneration and/or detachment, abnormal opsin localization, subretinal macrophage infiltration, and severely reduced retinal electrophysiological activity. The phenotype is associated with abnormal recycling endosomes in the RPE, and we speculate that this deficit impairs the ability of the RPE to fulfil one or more of its normal support functions (see below). A defect in

Investigative Ophthalmology & Visual Science

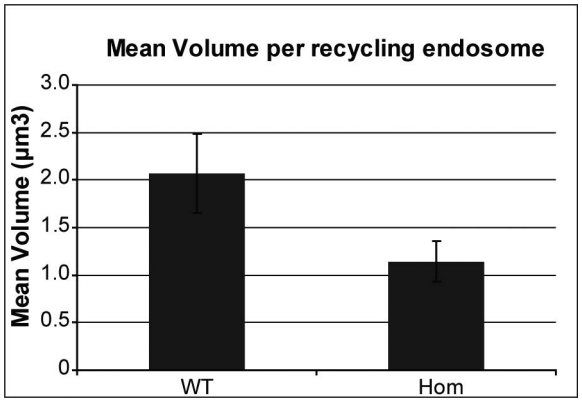

Figure 8. Loss of *Slc9a8* results in changes in recycling endosome morphology. Quantification of the mean volume of each recycling endosome in WT and *Slc9a8*$^{tm1a(KOMP)Wtsi}$ homozygous mutant mouse embryonic fibroblasts shows a statistically significant difference between WT and homozygous *Slc9a8*$^{tm1a(KOMP)Wtsi}$ (Hom). Unpaired Student's *t*-test, $^{*}P < 0.05$).

the ocular surface of *Slc9a8* KO mice has been reported recently, which results in decreased tear production and potential defects in ocular epithelial protection,[16] but we did not observe any morphological abnormalities of the cornea. The only other abnormal phenotype detected by the high-throughput screening performed at WTSI is male infertility. The fertility defect has been examined in detail recently, and appears to be associated with defects in luteinizing hormone receptor and a concomitant reduction in testosterone.[27]

Others have found that a gene-trap mutation of *Slc9a8* had defects in the gastrointestinal tract, including a reduction in the number of goblet cells, reduction in mucin production, and decreased surface pH along with an approximately 18% increase in length of the small intestine and a doubling in the weight of the cecum.[13] The reduction in mucin appeared to lead to an increase in bacteria attached to the distal colon and a sensitivity to dextran sulfate.[28] The mutant mice also had a higher incidence of gastric ulcers than controls.[15] None of these phenotypes was observed in the mice screened at WTSI, although the high-throughput nature of the screen meant that these parameters were not measured. Nevertheless, the mice had normal weight and growth. Furthermore, the mutant strain was subjected to bacterial challenge by intravenous infection with *Salmonella* and oral infection with *Citrobacter*, and showed no difference in infection. In particular following *Citrobacter* infection the colon and caecum were closely examined for bacterial load and for hyperplasia, and the mutant mice were no different from controls. It is worth noting that the genetic background of the two studies differ; in the previous studies the mutation was generated on a 129S1 background, but maintained on a mixed, outbred, 129/Black Swiss background, while in the current study the mutation was made and initially screened on a C57BL6/N background and subsequently maintained by backcrossing on to the closely related C57BL6/J strain.

Given the widespread expression of *Slc9a8* it is surprising that we detected no defects in any other systems, in particular in kidney function where the gene is expressed at higher levels and the protein is localized to the apical membrane of the proximal tubule.[14,12] The abundance of other NHE family members may mean that in most tissues there is sufficient function provided by other cotransporters to compensate for loss of NHE8.

Slc9a8 is Not Required for Maintenance of IOP

Maintenance of IOP requires sodium/hydrogen ion exchange. Aqueous humor is secreted by the ciliary epithelium and drains out at the iridocorneal angle through the trabecular meshwork into Schlemm's canal. The balance between secretion and drainage is the key factor in regulating the volume, and, hence, the pressure of the aqueous humor. Blockage of drainage is a common cause of raised IOP. Secretion of the aqueous humor must be tightly regulated to prevent over- or underproduction with consequential increase or decrease in volume and pressure. Avila et al.[3] showed that pharmacological inhibition of the sodium/hydrogen ion exchange protein NHE1 (SLC9A1) reduced IOP. As *Slc9a8* is expressed in the ciliary epithelium, and the activity of the drugs against this target was not characterized, it was reasonable to postulate that this protein might be the key cotransporter in the ciliary body regulating aqueous humor secretion, and that the retinal pathology we observe in the mutants might be a consequence of lowered IOP. However, we found no change in IOP measurements between mutant and control mice, indicating that NHE8 is not the prime regulator of IOP.

An RPE Defect Underlies the Eye Pathology

Cell-type specific knock-out of *Slc9a8* in only the RPE recapitulates the phenotype seen in a global knock-out, indicating that absence of the gene in the RPE is sufficient to cause the retinal defect. Histology reveals evidence of RPE cell death, shown by large multinucleated RPE cells in mutant mice, possibly caused by the compensatory expansion of cells to replace dying neighbor cells. Others have shown that NHE8 localizes to the trans Golgi network and to the endosomal compartment in HeLa cells,[5] and we confirmed this in RPE1 cells. Knockdown of NHE8 using siRNA in HeLa cells results in perinuclear clustering of recycling endosomes. We did not observe such clustering universally in fibroblasts from *Slc9a8* knockout mice, but we did see a significant decrease in the size of endosomes.

Lawrence et al.[5] do not report a pH change, and it is possible that cell types vary in their requirement of NHE8 in endosomes. Certainly, an endosomal defect may underlie the mutant phenotype we observed. Phagocytosis and recycling of photoreceptor outer segments is one of the key functions of the RPE and even a small deficiency in this function could result in abnormal photoreceptor function. This has been demonstrated in other mouse models of retinal degeneration, including the mouse myosin VIIa (*Myo7a*) mutant, which models Usher syndrome. The RPE of *Myo7a* null mice is unable to phagocytose photoreceptor outer segments efficiently and is thought to contribute to progressive blindness.[29] The NHE8 is not the first ion channel implicated in retinal degeneration. Bestrophin forms an oligomeric chloride channel on the basolateral membrane of the RPE cells and mutations in this gene cause various types of macular degeneration.[30–32] In particular, BEST1 mutant proteins exhibit chloride channel defects that underlie their degeneration phenotypes.[33] It is clear, therefore, that ion exchange in the RPE is important for RPE function, and disturbance in the process can result in disease.

Targeted knockout of another solute carrier gene, *Slc4a5*, shows a similar eye pathology to the one we described here.[34] The *Slc4a5* gene encodes an electrogenic sodium bicarbonate cotransporter that is necessary for normal function of the choroid plexus, and maintenance of cerebrospinal fluid composition and intracranial pressure. The eyes of these mutant mice have retinal detachment and a functional ERG deficit, similar to our *Slc9a8* mutant, but the critical cells through which the phenotype is mediated have not been identified.

Acknowledgments

We thank Craig Nicol for help with photography and illustrations, Iain McCall for animal husbandry, Simon John and Mimi de Vries for tonometry advice, Katherine Bowers (UCL, London, UK) for the NHE8-HA construct, Mark Handley (MRC Human Genetics Unit) for the GalT-GFP, and the Research Support Facility and Mouse Informatics Group of WTSI for their excellent technical support.

Supported by funding from the Medical Research Council, Fight for Sight, the Royal College of Surgeons Edinburgh, the Wellcome Trust (Grant 079643), and the European Mouse Disease Clinic (EUMODIC), an EU Integrated Research Programme.

Disclosure: **S. Jadeja**, None; **A.R. Barnard**, None; **L. McKie**, None; **S.H. Cross**, None; **J.K. White**, None; **M. Robertson**, None; **P.S. Budd**, None; **R.E. MacLaren**, None; **I.J. Jackson**, None

References

1. White JK, Gerdin AK, Karp NA, et al. Genome-wide generation and systematic phenotyping of knockout mice reveals new roles for many genes. *Cell*. 2013;154:452–464.
2. Donowitz M, Ming Tse C, Fuster D. SLC9/NHE gene family, a plasma membrane and organellar family of Na(+)/H(+) exchangers. *Mol Aspects Med*. 2013;34:236–251.
3. Avila MY, Seidler RW, Stone RA, Civan MM. Inhibitors of NHE-1 Na+/H+ exchange reduce mouse intraocular pressure. *Invest Ophthalmol Vis Sci*. 2002;43:1897–1902.
4. Brett CL, Tukaye DN, Mukherjee S, Rao R. The yeast endosomal Na+K+/H+ exchanger Nhx1 regulates cellular pH to control vesicle trafficking. *Mol Biol Cell*. 2005;16:1396–1405.
5. Lawrence SP, Bright NA, Luzio JP, Bowers K. The sodium/proton exchanger NHE8 regulates late endosomal morphology and function. *Mol Biol Cell*. 2010;21:3540–3551.
6. Cox GA, Lutz CM, Yang CL, et al. Sodium/hydrogen exchanger gene defect in slow-wave epilepsy mutant mice. *Cell*. 1997;91:139–148.
7. Bell SM, Schreiner CM, Schultheis PJ, et al. Targeted disruption of the murine Nhe1 locus induces ataxia, growth retardation, and seizures. *Am J Physiol*. 1999;276:C788–C795.
8. Ouyang Q, Lizarraga SB, Schmidt M, et al. Christianson syndrome protein NHE6 modulates TrkB endosomal signaling required for neuronal circuit development. *Neuron*. 2013;80:97–112.
9. Schultheis PJ, Clarke LL, Meneton P, et al. Targeted disruption of the murine Na+/H+ exchanger isoform 2 gene causes reduced viability of gastric parietal cells and loss of net acid secretion. *J Clin Invest*. 1998;101:1243–1253.
10. Schultheis PJ, Clarke LL, Meneton P, et al. Renal and intestinal absorptive defects in mice lacking the NHE3 Na+/H+ exchanger. *Nature Genet*. 1998;19:282–285.
11. Gawenis LR, Greeb JM, Prasad V, et al. Impaired gastric acid secretion in mice with a targeted disruption of the NHE4 Na+/H+ exchanger. *J Biol Chem*. 2005;280:12781–12789.
12. Goyal S, Vanden Heuvel G, Aronson PS. Renal expression of novel Na+/H+ exchanger isoform NHE8. *Am J Physiol Renal Physiol*. 2003;284:F467–F473.
13. Xu H, Zhang B, Li J, Wang C, Chen H, Ghishan FK. Impaired mucin synthesis and bicarbonate secretion in the colon of NHE8 knockout mice. *Am J Physiol Gastrointest Liver Physiol*. 2012;303:G335–G343.
14. Becker AM, Zhang J, Goyal S, et al. Ontogeny of NHE8 in the rat proximal tubule. *Am J Physiol Renal Physiol*. 2007;293:F255–F261.
15. Xu H, Li J, Chen H, Wang C, Ghishan FK. NHE8 plays important roles in gastric mucosal protection. *Am J Physiol Gastrointest Liver Physiol*. 2013;304:G257–G261.
16. Xu H, Zhao Y, Li J, et al. Loss of NHE8 expression impairs ocular surface function in mice. *Am J Physiol Cell Physiol*. 2014;308:C79–C87.
17. Kleinjan DA, Seawright A, Mella S, et al. Long-range downstream enhancers are essential for Pax6 expression. *Dev Biol*. 2006;299:563–581.
18. Delmas V, Martinozzi S, Bourgeois Y, Holzenberger M, Larue L. Cre-mediated recombination in the skin melanocyte lineage. *Genesis*. 2003;36:73–80.
19. Muzumdar MD, Tasic B, Miyamichi K, Li L, Luo L. A global double-fluorescent Cre reporter mouse. *Genesis*. 2007;45:593–605.
20. Wallace HA, Marques-Kranc F, Richardson M, et al. Manipulating the mouse genome to engineer precise functional syntenic replacements with human sequence. *Cell*. 2007;128:197–209.
21. Schneider CA, Rasband WS, Eliceiri KWNIH. Image to ImageJ: 25 years of image analysis. *Nat Methods*. 2012;9:671–675.
22. Haddadin RI, Oh DJ, Kang MH, et al. Thrombospondin-1 (TSP1)-null and TSP2-null mice exhibit lower intraocular pressures. *Invest Ophthalmol Vis Sci*. 2012;53:6708–6717.
23. Skarnes WC, Rosen B, West AP, et al. A conditional knockout resource for the genome-wide study of mouse gene function. *Nature*. 2011;474:337–342.
24. Aleman TS, Cideciyan AV, Aguirre GK, et al. Human CRB1-associated retinal degeneration: comparison with the rd8 Crb1-mutant mouse model. *Invest Ophthalmol Vis Sci*. 2011;52:6898–6910.
25. Mattapallil MJ, Wawrousek EF, Chan CC, et al. The Rd8 mutation of the Crb1 gene is present in vendor lines of C57BL/6N mice and embryonic stem cells, and confounds ocular induced mutant phenotypes. *Invest Ophthalmol Vis Sci*. 2012;53:2921–2927.
26. Longbottom R, Fruttiger M, Douglas RH, Martinez-Barbera JP, Greenwood J, Moss SE. Genetic ablation of retinal pigment epithelial cells reveals the adaptive response of the epithelium and impact on photoreceptors. *Proc Natl Acad Sci U S A*. 2009;106:18728–18733.
27. Xu H, Chen H, Li J, Zhao Y, Ghishan FK. Disruption of NHE8 Expression Impairs Leydig cell function in the testes. *Am J Physiol Cell Physiol*. 2014;308:C330–C338.
28. Liu C, Xu H, Zhang B, et al. NHE8 plays an important role in mucosal protection via its effect on bacterial adhesion. *Am J Physiol Cell Physiol*. 2013;305:C121–128.
29. Gibbs D, Kitamoto J, Williams DS. Abnormal phagocytosis by retinal pigmented epithelium that lacks myosin VIIa, the Usher syndrome 1B protein. *Proc Natl Acad Sci U S A*. 2003;100:6481–6486.
30. Petrukhin K, Koisti MJ, Bakall B, et al. Identification of the gene responsible for Best macular dystrophy. *Nat Genet*. 1998;19:241–247.
31. Marquardt A, Stohr H, Passmore LA, Kramer F, Rivera A, Weber BH. Mutations in a novel gene, VMD2, encoding a protein of unknown properties cause juvenile-onset vitelliform macular dystrophy (Best's disease). *Hum Mol Genet*. 1998;7:1517–1525.
32. Kramer F, White K, Pauleikhoff D, et al. Mutations in the VMD2 gene are associated with juvenile-onset vitelliform macular dystrophy (Best disease) and adult vitelliform macular dystrophy but not age-related macular degeneration. *Eur J Hum Genet*. 2000;8:286–292.
33. Yu K, Qu Z, Cui Y, Hartzell HC. Chloride channel activity of bestrophin mutants associated with mild or late-onset macular degeneration. *Invest Ophthalmol Vis Sci*. 2007;48:4694–4705.
34. Kao L, Kurtz LM, Shao X, et al. Severe neurologic impairment in mice with targeted disruption of the electrogenic sodium bicarbonate cotransporter NBCe2 (Slc4a5 gene). *J Biol Chem*. 2011;286:32563–32574.

Investigative Ophthalmology & Visual Science